

Supporting Information

General synthesis of single atom electrocatalysts via a facile condensation-carbonization process

Weiming Chen, Xuanli Luo, Thomas J A Slater, Yongfang Zhou, Sanliang Ling, Rui Bao, Jesum Alves Fernandes, Jianshe Wang and Yi Shen*

Mr. W. Chen, Miss Y. Zhou and Dr Y. Shen School of Food Science and Engineering, South China University of Technology, Guangzhou 510641, China. Email: feyshen@scut.edu.cn (Y. S.)

Dr Y. Shen, Overseas Expertise Introduction Center for Discipline Innovation of Food Nutrition and Human Health (111 Center), Guangzhou, 510641, China

Dr X. Luo and Dr S. Ling Advanced Materials Research Group, Faculty of Engineering, University of Nottingham, Nottingham, NG7 2RD, UK

Dr T. Slater, Electron Physical Sciences Imaging Centre, Diamond Light Source Ltd., Oxfordshire OX11 0DE, United Kingdom

Dr R. Bao, Kunming University of Science and Technology, Kunming, xxx, China.

Dr J. Alves Fernandes, School of Chemistry, University of Nottingham, Nottingham, UK

Dr J. Wang, School of Chemical Engineering and Energy, Zhengzhou University, Zhengzhou 450001, China

Table of Contents

Experimental section.....	S3-4
Table S1-2 XPS and ICP-AES analysis results.....	S5
Table S3 Contents of N species.....	S6
Table S4 EXAFS fitting result.....	S7
Table S5 Comparison of glycerol electro-oxidation activity	S8
Table S6 Comparison of OER activity	S9
Table S7 Comparison of overall efficiency.....	S10
Fig. S1 FTIR spectra of the samples.....	S11
Fig. S2 Structure Characterization of Pt/NCNSs.....	S12
Fig. S3 XRD spectra of the samples.....	S13
Fig. S4 Raman spectra of the samples.....	S14
Fig. S5-12 Raman spectra of the samples.....	S15-22
Fig. S13-18 XPS of the samples.....	S23-28
Fig. S19-21 XAFS of the samples.....	S29-31
Fig. S22 CV of glycerol oxidation over the Pd/NCNSs.....	S32
Fig. S23 Additional two adsorption configurations of Au/NCNSs.....	S33
Fig. S24 CV of glycerol oxidation over the Au/NCNSs samples.....	S34-35
Fig. S25 Cycle activity of Au/NCNSs.....	S36
Fig. S26-28 LSV and overpotential of OER over the Ni/NCNSs.....	S36-38
Fig. S29-31 OER performance (TOF values and chronoamperometric curves) of the samples.....	S39-41
Fig. S32 HAADF-STEM images of spent Co/NCNSs.....	S42
Fig. S33 HAADF-STEM images of spent Au/NCNSs.....	S43
Fig. S34-35 C_{dl} value of the samples.....	S44-45
Fig. S36-39 HER performance (LSV, overpotentials, Tafel slopes and TOF values) of the samples.....	S46-49
Fig. S40 Digital photos of solar panel powered set-up electrolysis.....	S50

Fig. S41 Digital photo of a 2.0 V solar panel.....S51

References.....S52

Experimental section

Materials

Furfural (C₅H₄O₂) was purchased from McLean Biochemical Technology Co. LTD. (Shanghai, China), Cyanamide (CH₂N₂, 50 wt% in aqueous) was purchased from Aladdin Co. LTD. (Shanghai, China), Hydrochloric acid was provided by Nanjing Chemical Reagent Co. LTD. (Nanjing, China), Ferric chloride hexahydrate (FeCl₃·6H₂O), Cobalt chloride hexahydrate (CoCl₂·6H₂O) and Nickel chloride hexahydrate (NiCl₂·6H₂O) were provided by Guangzhou Chemical Reagent Co. LTD. (Guangzhou, China), Tianjin Kemeiou Chemical Reagent Co. LTD. (Tianjin, China) and Damao Chemical Reagent Co. LTD. (Tianjin, China), respectively. Chloroplatinic acid hexahydrate (H₂PtCl₆·6H₂O), Tetrachlorogold trihydrate (AuCl₄·3H₂O), Palladium chloride (PdCl₂) was purchased from Sigma-Aldrich (Shanghai, China). Nafion solution (5 wt.%) was purchased from the Sunlaite Co. Ltd. (Kunshan, China). Isopropanol and ethylene glycol were provided by the Qiangsheng Chemical Reagent Co. Ltd. (Jiangsu, China) and Fuyu Chemical Reagent Co. Ltd. (Tianjin, China), respectively. All the chemicals were of analytic grade and were used as received without further purification.

Theoretical density of single platinum atom in the Pt/NCNSs sample (C_{Pt})

The theoretical density of platinum atom in the Pt/NCNSs sample was calculated by:

$$C_{Pt} = \frac{N}{V}$$

Where V is the volume of Pt/NCNSs sample, and N is the number of single platinum atom in a sample volume of V.

Based on following equations, C_{Pt} (nm⁻³) can be calculated:

$$\begin{aligned} C_{Pt} &= \frac{\text{Pt wt\%} \times \rho \text{ (g cm}^{-3}\text{)}}{M_{Pt} \text{ (g mol}^{-1}\text{)}} \times N_A \text{ (mol}^{-1}\text{)} \times \left(\frac{1 \text{ (cm)}}{10^7 \text{ (nm)}} \right)^3 = \frac{\text{Pt wt\%} \times \rho \text{ (g cm}^{-3}\text{)}}{0.324 \text{ (g)}} \times \frac{\text{cm}^3}{\text{nm}^3} \\ &= \frac{1.73 \times 10^{-2} \times 2.0 \text{ (g cm}^{-3}\text{)}}{0.324 \text{ (g)}} \times \frac{\text{cm}^3}{\text{nm}^3} = 0.1068 \text{ nm}^{-3} \approx 0.11 \text{ nm}^{-3} \end{aligned}$$

Where Pt wt% is the loading of platinum in Pt/NCNSs, ρ is the density of the Pt/NCNSs sample, and M_{Pt} is the molar mass of platinum. Since the major content of the sample is carbon (over 95 wt%), the density of the Pt/NCNSs can be equivalent to that of carbon

material. According to Raman and XRD results, both graphitized carbon (2.25 g cm⁻³) and amorphous carbon (1.80 g cm⁻³) were present in the sample. Therefore, the density of the Pt/NCNSs sample was estimated as 2.0 g cm⁻³.

Energy efficiency of solar-to-hydrogen (η)

Energy Efficiency of solar-to-hydrogen was calculated by:

$$\eta (\%) = \frac{E_h}{E_0} \times 100\%$$

Where E_h is the energy of the hydrogen produced by electrolysis, and E_0 is the overall solar energy input on the solar panel.

Based on following equations, E_h can be calculated:

$$\begin{aligned} \text{H}_2 (\text{g}) + \frac{1}{2} \text{O}_2 (\text{g}) &= \text{H}_2\text{O} (\text{l}), \Delta H = -285.8 \text{ KJ mol}^{-1} \\ E_h &= \frac{V_h (\text{mL})}{22400 (\text{mL mol}^{-1})} \times \frac{273 (\text{K})}{T (\text{K})} \times (-\Delta H) (\text{kJ mol}^{-1}) \\ &= \frac{10.1 (\text{mL})}{22400 (\text{mL mol}^{-1})} \times \frac{273 (\text{K})}{303 (\text{K})} \times 285.8 (\text{kJ mol}^{-1}) = 0.116 \text{ kJ} = 116 \text{ J} \end{aligned}$$

Where V_h is the volume of hydrogen obtained from anode, and T is the environment temperature.

$$\begin{aligned} E_0 &= S (\text{m}^2) \times \int_0^t P(t) (\text{W m}^{-2}) \bullet dt (\text{s}) = 0.04^2 (\text{m}^2) \times \int_0^{2130} P(t) (\text{W m}^{-2}) \bullet dt (\text{s}) \\ &= 0.04^2 (\text{m}^2) \times E_t (\text{J m}^{-2}) = 0.04^2 (\text{m}^2) \times 823300 (\text{J m}^{-2}) = 1317 \text{ J} \end{aligned}$$

Where S is the area of solar panel, $P(t)$ is the power density of the sunlight in real time, and E_t is the energy density of sunlight during the electrolysis process

$$\eta (\%) = \frac{E_h}{E_0} \times 100\% = \frac{116 (\text{J})}{1317 (\text{J})} \times 100\% = 8.8\%$$

In the overall water splitting system, Ni/NCNSs and Co/NCNSs was utilized as anodic and cathodic electrocatalysts, the area of both anodic and cathodic was $10 \times 10 \text{ mm}$, and the loading of the electrocatalysts was 0.128 mg cm^{-2} . The electrolyte was 1 M KOH and a 2.0 V solar panel ($40 \times 40 \text{ mm}$) was utilized as power supply (**Fig. S41**, ESI†). The power density of the sunlight was recorded at intervals of 5 seconds by a power meter, and hydrogen and oxygen were collected by a device shown in Fig. 4h

and S37. The environment temperature (T) was 303 K. After 2130 seconds, 5.2 mL of oxygen and 10.1 mL (V_h) of hydrogen were obtained from the cathode and anode, respectively. The power density of the sunlight was shown in inset of **Fig. 5e**.

The TOF values of the catalysts were calculated based on Li's work.¹

Table S1 XPS analysis results of the samples

Number	Sample	C (wt%)	N (wt%)	Metal (wt%)	O (wt%)
1	Fe/NCNSs	91.38	1.74	1.52	5.35
2	Co/NCNSs	85.70	2.96	1.25	10.08
3	Ni/NCNSs	83.94	2.40	2.35	11.31
4	Ni/NCNSs-800	81.12	3.61	1.00	15.28
5	Ni/NCNSs-1000	91.19	1.98	1.72	5.11
6	Ni/NCNSs-1100	83.99	0.74	0.04	15.23
7	Pt/NCNSs	94.96	3.31	1.73	--
8	Au/NCNSs	78.21	7.86	2.28	10.90
9	Pd/NCNSs	85.69	5.67	0.93	7.70

Table S2 Metal loadings in the resulting catalysts

Sample	Metal loading from XPS results (wt.%)	Metal loading from ICP-AES results (wt.%)
Pt/NCNSs	1.73	1.79
Au/NCNSs	2.28	2.41
Pd/NCNSs	0.93	1.66
Fe/NCNSs	1.52	1.72
Co/NCNSs	1.25	1.62

Ni/NCNSs	2.35	2.33
----------	------	------

Table S3 Contents of N species of the samples based on the N 1s spectra.

Catalysts	Pyridinic-N (%)	M-N _x (%)	Pyrrolic-N (%)	Graphitic-N (%)	Oxidized-N (%)	Total N-content (wt %)
Ni/NCNSs-800	30.0	6.6	20.5	28.8	14.1	3.61
Ni/NCNSs	22.2	16.4	18.0	30.1	13.2	2.40
Ni/NCNSs-1000	21.7	16.6	20.1	31.7	10.0	1.98
Ni/NCNSs-1100	22.5	15.7	11.2	24.0	26.7	0.74
Co/NCNSs	20.1	10.7	22.9	23.5	22.7	2.96
Fe/NCNSs	18.3	9.6	36.6	20.7	14.8	1.74
Pt/NCNSs	25.1	15.7	22.0	23.5	13.7	3.31
Au/NCNSs	29.6	15.6	17.7	19.1	18.0	7.86
Pd/NCNSs	22.4	14.8	14.4	33.2	15.2	5.67

Table S4 Structural parameters obtained from the EXAFS fitting analysis

S_0^2	Sample	Path	^a C.N.	^b R (Å)	^c $\sigma^2 \times 10^{-3}$ (Å ²)	^d ΔE_0 (eV)	R factor
0.78	Fe foil	Fe-Fe	8*	2.48±0.01	5.2±0.6	7.4±1.1	0.001
		Fe-Fe	6*	2.84±0.01	6.8±1.4	5.7±2.2	
	Fe/NCNSs	Fe-N	3.7±0.8	2.17±0.02	13.9±2.5	5.2±1.6	0.006
		Fe-O	2.2±0.6	2.00±0.04	3.0±1.2	-8.9±5.3	
		Fe-Fe	1.2±0.2	2.74±0.01	9.2±3.6	-5.7±5.3	
0.80	Ni foil	Ni-Ni	12*	2.48±0.01	6.1±0.2	6.8±0.4	0.001
	Ni/NCNSs	Ni-N	4.3±1.8	1.87±0.03	16.2±4.6	-15.2±5.2	0.015
0.82	Pd foil	Pd-Pd	12*	2.74±0.01	5.2±0.3	-5.5±0.5	0.002
	Pd/NCNSs	Pd-N	2.9±1.1	2.13±0.04	11.7±8.9	7.0±3.4	0.014
		Pd-Pd	4.0±1.4	2.83±0.01	9.2±2.6	-5.3±2.4	
0.84	Pt foil	Pt-Pt	12*	2.76±0.01	4.7±0.2	8.8±0.4	0.001
	Pt/NCNSs	Pt-N	3.0±0.6	2.00±0.02	6.0±2.4	7.5±2.6	0.019

^aN: coordination numbers; ^bR: bond distance; ^c σ^2 : Debye-Waller factors; ^d ΔE_0 : the inner potential correction. R factor: goodness of fit. * the experimental EXAFS fit of metal foil by fixing CN as the known crystallographic value.

The obtained XAFS data was processed in Athena (version 0.9.25) for background, pre-edge line and post-edge line calibrations. Then Fourier transformed fitting was carried out in Artemis (version 0.9.25). The k^3 weighting, k-range of 3 - 12 Å⁻¹ and R range of 1 - ~3 Å were used for the fitting. The four parameters, coordination number, bond length, Debye-Waller factor and E_0 shift (CN, R, σ^2 , ΔE_0) were fitted without anyone was fixed, constrained, or correlated.

Table S5 Comparison on glycerol electro-oxidation activity of the electrocatalysts.

References	Catalyst	Loading density ($\text{mg}_{\text{cat}} \text{cm}^{-2}$)	Activity $\text{mA mg}_{\text{noble metal}}^{-1}$	Electrolyte
Our work	Pt-NCNSs	0.113	5300	0.5 M KOH + 0.5 M Glycerol
	Au-NCNSs	0.113	3640	
	Pd-NCNSs	0.113	730	
<i>ACS Catal.</i> , 2015, 5, 3174.	Pd-CB	1.0	900	0.5 M NaOH + 0.5 M Glycerol
	Pd-CN _x	1.0	1050	
	Pd-CN _x /G	1.0	1100	
<i>Energy Environ. Sci.</i> , 2015, 8, 2910.	Pd ₅₅ Pt ₃₀	0.025	1800	1 M KOH + 0.1 M Glycerol
<i>Energy Environ. Sci.</i> , 2016, 9, 3097.	Pd ₆₂ Au ₂₁ Ni ₁₇	0.014	3300	1 M KOH + 0.1 M Glycerol
<i>J. Am. Chem. Soc.</i> , 2014, 136, 3937.	Pd ₄ Bi	0.2	700	1 M KOH + 0.1 M Glycerol
	Pd ₆ Bi	0.2	550	
<i>Green Chem.</i> , 2015, 18, 386.	Pt/Ag@C	0.86	1080	1 M KOH + 0.1 M Glycerol
	Pt/MWCNT	0.86	240	
<i>Adv. Mater.</i> , 2019, 31, 1804763.	Pt-in-GN	1	600	1 M KOH + 0.1 M Glycerol
	Pt-in-VGCC	0.05 (Pt)	1280	
<i>J. Mater. Chem. A</i> , 2017, 5, 15932.	Au ₁ Cu ₁	0.06 (Au)	2260	1 M KOH + 1 M Glycerol
<i>Electrochem. Commun.</i> , 2014, 46, 36.	PtAgNTs	0.1 (Pt)	1600	0.5 M NaOH + 0.5 M Glycerol
	PtNTs	0.1 (Pt)	1050	
<i>Applied Catal. B: Environ.</i> , 2015, 176-177, 429.	Pd ₁ Sn ₁	0.2	1050	1 M KOH + 0.1 M Glycerol
<i>Nanoscale</i> , 2018, 10, 16468.	Pt ₃ FeNWs	0.03 (Pt)	2000	1 M KOH + 1 M Glycerol
<i>ACS Appl. Mater. Interfaces</i> , 2018, 10, 12659.	Pd ₂ Pb NCs	0.1	2220	1 M KOH + 1 M Glycerol
<i>J. Mater. Chem. A</i> 2015, 3, 15920.	Pd ₆₃ Ag ₃₇ nanocorals	0.085	1600	1 M KOH + 0.5 M Glycerol
<i>Chem. Eng. J.</i> 2017, 38, 419.	Pd-NiO _x -P/C	0.2	380	0.1 M KOH + 0.5 M Glycerol

Table S6 Comparison on OER activity of the electrocatalysts.

References	Catalyst	Loading density (mg cm ⁻²)	Overpotential at 10 mA cm ⁻² (V)	Electrolyte
This work	Ni/NCNSs Co/NCNSs	0.128 mg cm⁻² 0.128 mg cm⁻²	1.53 1.57	1.0 M KOH
<i>Nat. Catal.</i> , 2018, 1, 63	Ni–NHGF	0.275 mg cm ⁻²	1.56	1.0 M KOH
<i>Angew. Chem. Int. Ed.</i> , 2018, 57, 1856	FeCo-N _x -CN	0.10 mg cm ⁻²	1.60	1.0 M KOH
<i>J. Am. Chem. Soc.</i> , 2017, 139, 3336	Co–C ₃ N ₄ /CNT	2.0 mg cm ⁻²	1.61	1.0 M KOH
<i>Nat. Commun.</i> , 2019, 10, 1392	S NiN _x -PC/EG	0.15 mg cm ⁻²	1.51	1.0 M KOH
<i>Sci. Adv.</i> , 2016, 2, e1501122	N-GRW	0.50 mg cm ⁻²	1.59	1.0 M KOH
<i>Nat. Energy</i> , 2016, 1, 15006	NCNTFs	0.20 mg cm ⁻²	1.60	1.0 M KOH
<i>Adv. Mater.</i> , 2017, 29, 1604480	Co–N _x P- GC/FEG	0.12 mg cm ⁻²	1.55	1.0 M KOH
<i>Angew. Chem. Int. Ed.</i> , 2017, 56, 610	S, N-Fe/N/C- CNT	0.60 mg cm ⁻²	1.60	0.1 M KOH
<i>Angew. Chem. Int. Ed.</i> , 2018, 57, 3514	CoSSPIL/CNT	0.05 mg cm ⁻²	1.64	0.1 M KOH
<i>Adv. Funct. Mater.</i> , 2015, 25, 872	N/Co-doped PCP//NRGO	0.714 mg cm ⁻²	1.66	0.1 M KOH
<i>Adv. Energy Mater.</i> , 2015, 5, 1401660	Ni@NC	0.40 mg cm ⁻²	1.62	0.1 M KOH
<i>J. Am. Chem. Soc.</i> , 2018, 140, 2610.	CoP/NCNHP	0.628 mg cm ⁻²	1.54	1.0 M KOH
<i>J. Am. Chem. Soc.</i> , 2017, 139, 3336.	Co-g- C ₃ N ₄ /CNT	0.196 mg cm ⁻²	1.61	1.0 M KOH
<i>Angew. Chem. Int. Ed.</i> , 2017, 129, 3955.	NiCoP/C nanoboxes	0.15 mg cm ⁻²	1.56	1.0 M KOH

Table S7 Comparison of overall solar-to-hydrogen conversion efficiency in recent reports.

References	Electrochemical cell	Solar cell	Efficiency	Electrolyte
This work	Ni/NCNSs // Co/NCNSs	Silicon	8.8%	1 M KOH
J. Am. Chem. Soc. 2015, 137, 14305.	CoMnO@CN (both sides)	A commercial planar Si solar cell module (Voc = 2.36)	8.0%	1 M KOH
Adv. Funct. Mater., 2016, 26, 8555	CuCoO-NW (both sides)	Silicon	4.5%	1 M KOH
Adv. Mater., 2016, 28, 3366	Ni // Pt	PBDTTPD:PCBM/PEDOT:PSS 3jn	6.1%	1 M NaOH
Proc. Natl. Acad. Sci. U.S.A., 2014, 111, 14057	NiBi // NiMoZn	c-Si 4p	10.0%	0.5 M KBi, (pH 9.2)
Science, 2014, 345, 1593	NiFe LDH // NiFe LDH	Lead halide (CH ₃ NH ₃ PbI ₃) perovskite 2p	12.3%	1 M NaOH
Energy Environ. Sci., 2013, 6, 3676	Pt // Pt	CuInGaSe ₂ 3p	10.5%	3 M H ₂ SO ₄ (pH 1.0)
Science, 2011, 334, 645	Co // NiMoZn	3jn-a-Si (wired device)	4.7%	0.5 M KBi (pH 9.2)

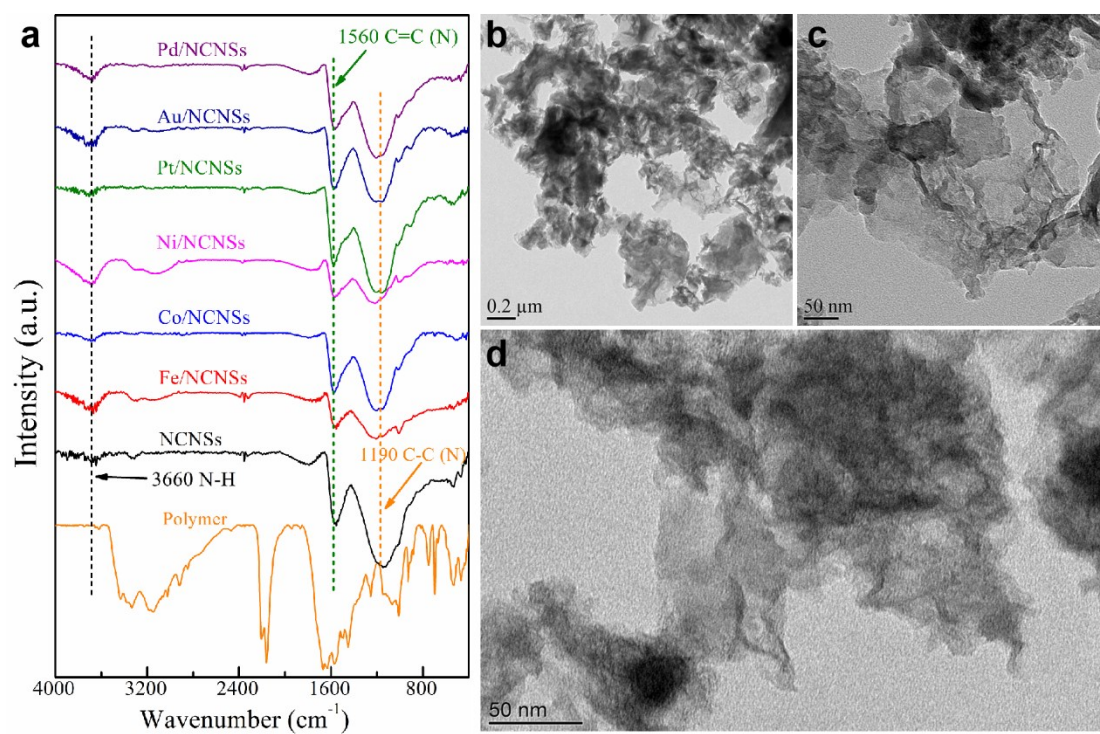


Fig. S1 (a) FTIR spectra of the samples and TEM images of (b) Fe/NCNSs, (c) Pt/NCNSs and (d) Co/NCNSs.

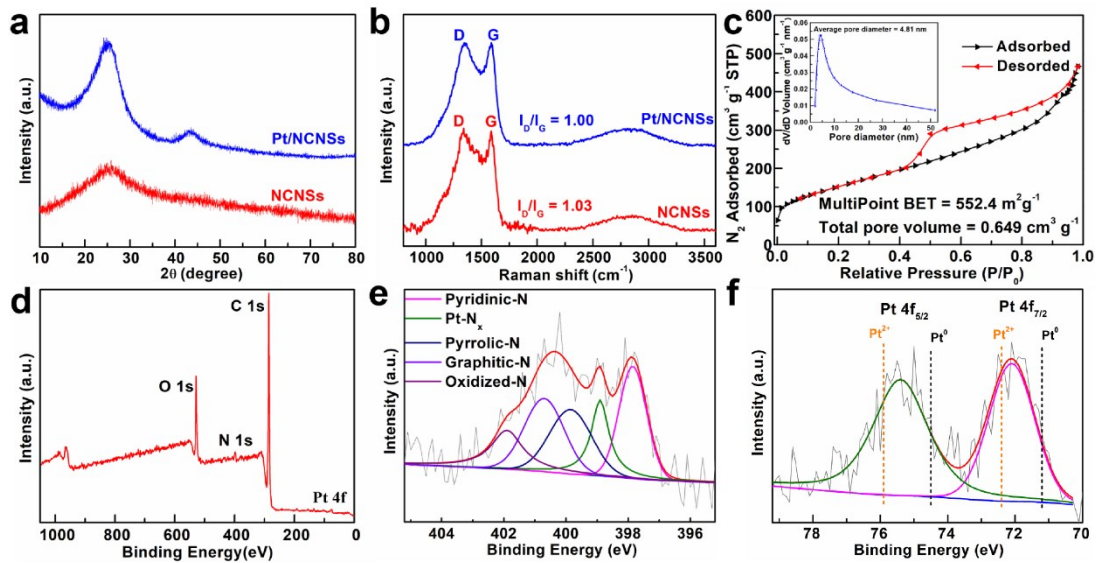


Fig. S2 Structural characterization. (a) XRD patterns and (b) Raman spectra of Pt/NCNSs and NCNSs, (c) N₂ adsorption-desorption isotherms of Pt/NCNSs, (d) XPS survey spectrum, (e) N 1s spectrum and (f) Pt 4f spectrum of Pt/NCNSs.

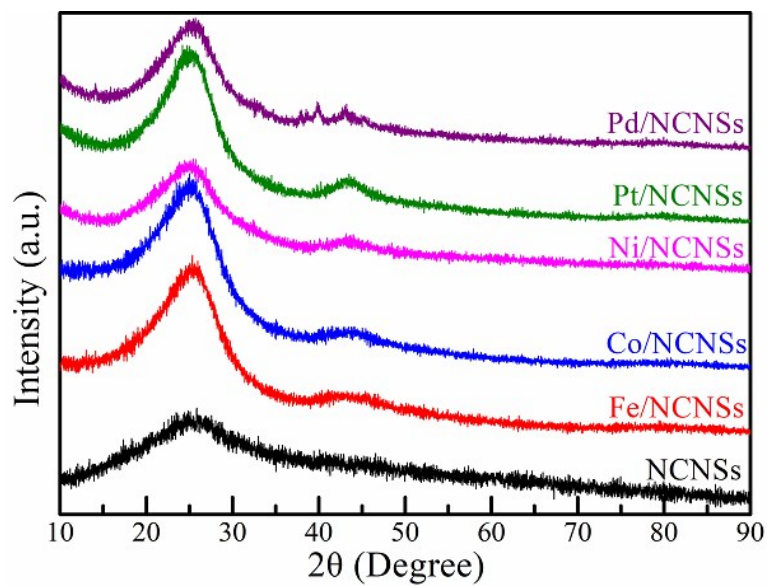


Fig. S3 XRD patterns of the samples

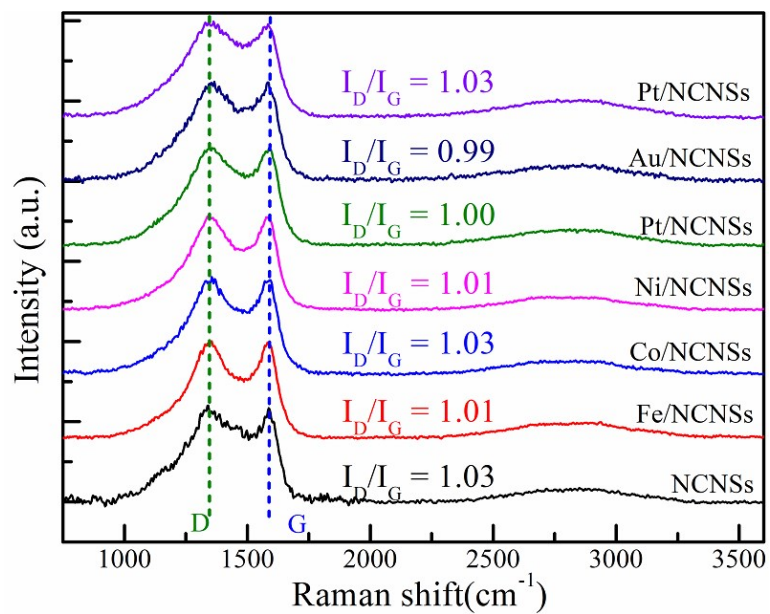


Fig. S4 Raman spectra of the samples

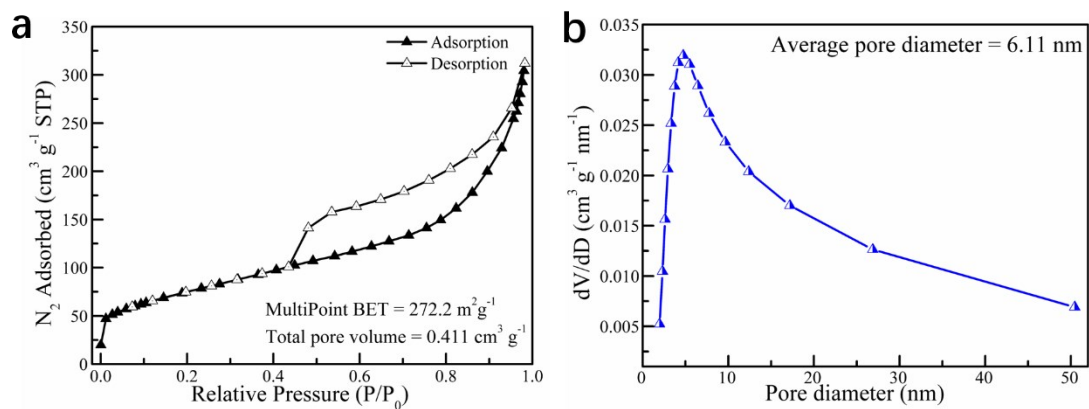


Fig. S5 (a) N₂ adsorption-desorption isotherm of the NCNSs and (b) corresponding pore size distribution.

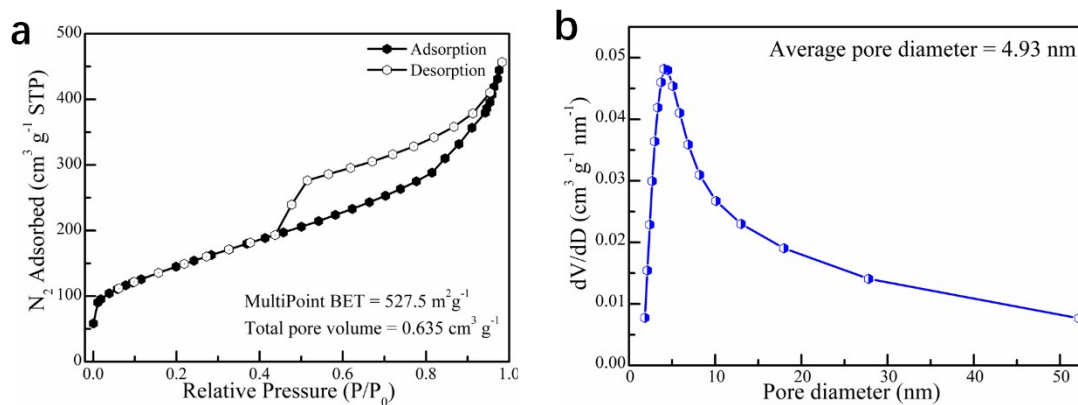


Fig. S6 (a) N_2 adsorption-desorption isotherm of the Au/NCNSs and (b) corresponding pore size distribution.

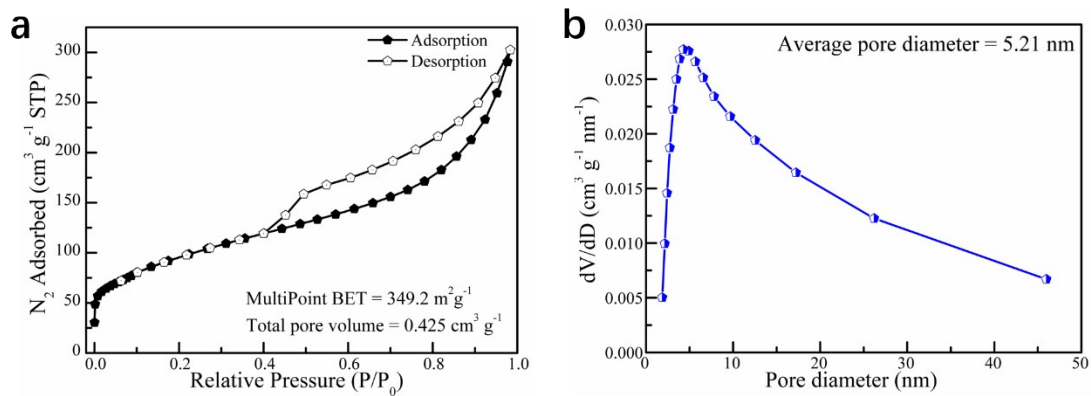


Fig. S7 (a) N_2 adsorption-desorption isotherm of the Pd/NCNSs and (b) corresponding pore size distribution.

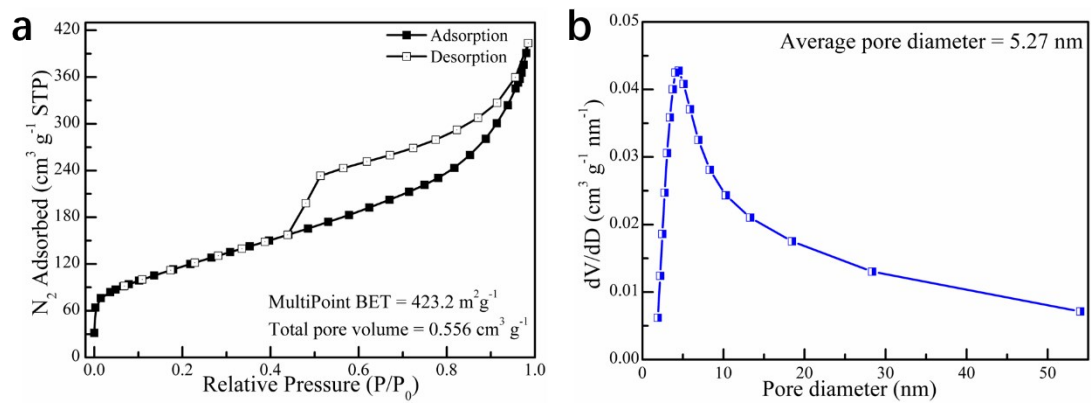


Fig. S8 (a) N_2 adsorption-desorption isotherm of the Co/NCNSs and (b) corresponding pore size distribution.

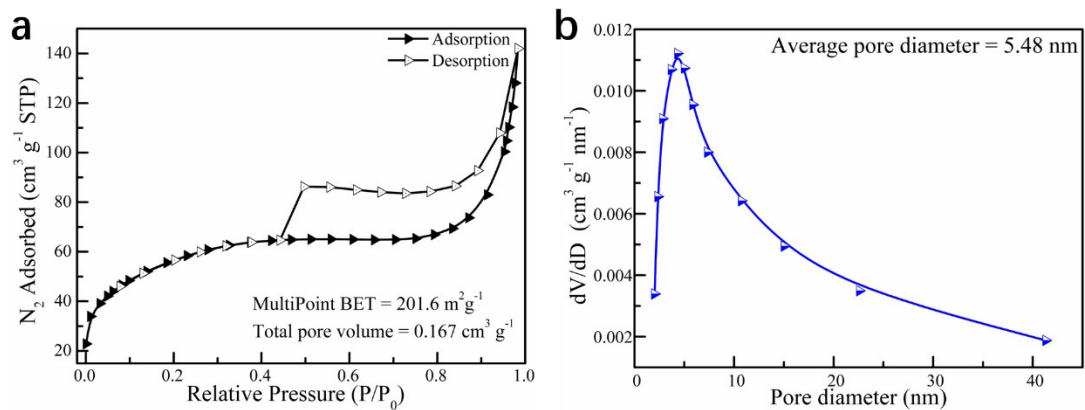


Fig. S9 (a) N_2 adsorption-desorption isotherm of the Fe/NCNSs and (b) corresponding pore size distribution.

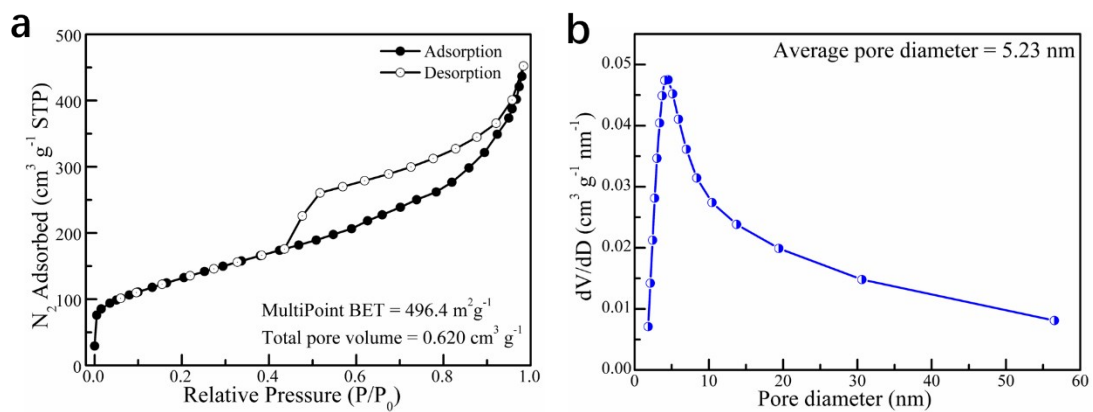


Fig. S10 (a) N₂ adsorption-desorption isotherm of the Ni/NCNSs and (b) corresponding pore size distribution.

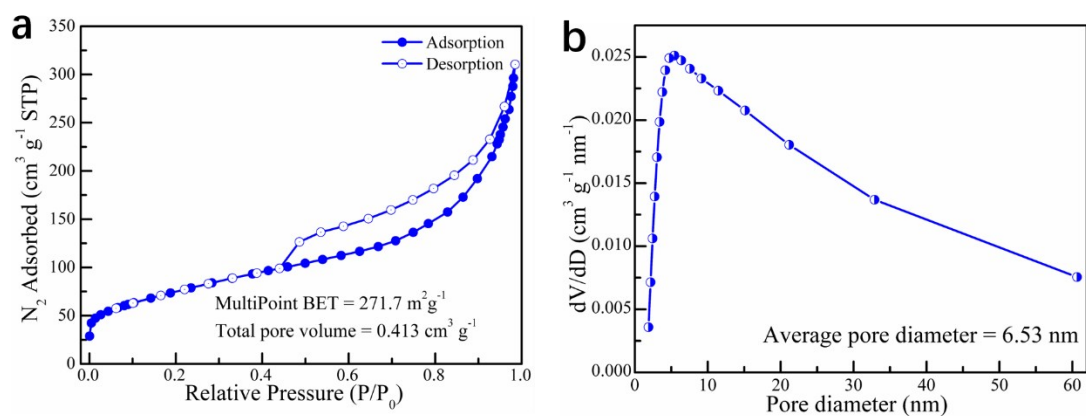


Fig. S11 (a) N₂ adsorption-desorption isotherm of the Ni/NCNSs-1000 and (b) corresponding pore size distribution.

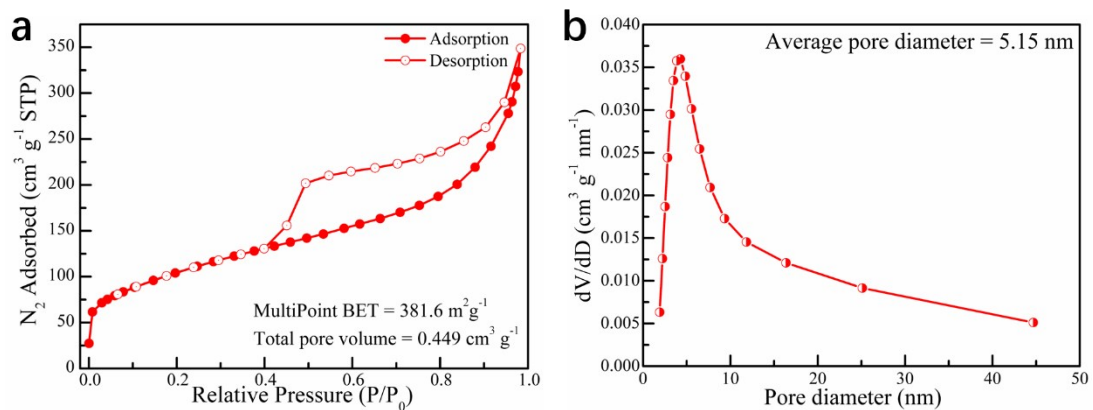


Fig. S12 (a) N_2 adsorption-desorption isotherm of the Ni/NCNSs-800 and (b) corresponding pore size distribution.

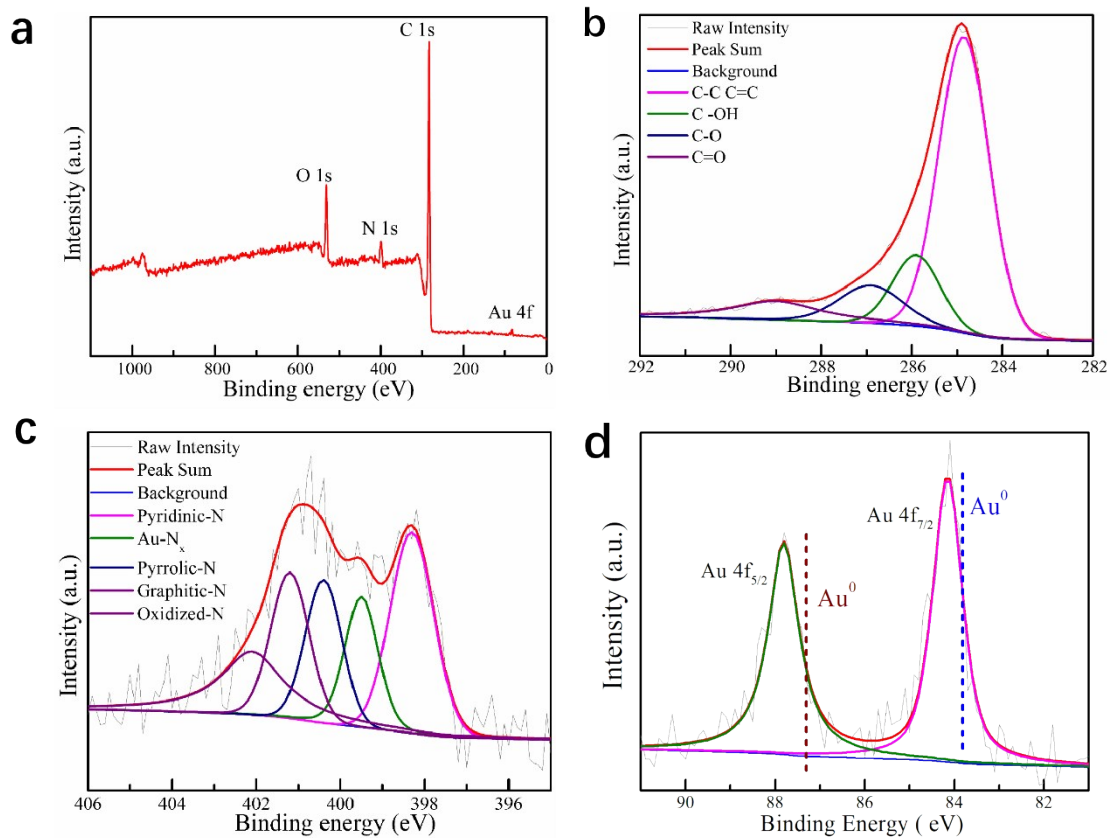


Fig. S13 (a) Survey, (b) C 1s, (c) N 1s and (d) Au 4f spectra of the Au/NCNSs.

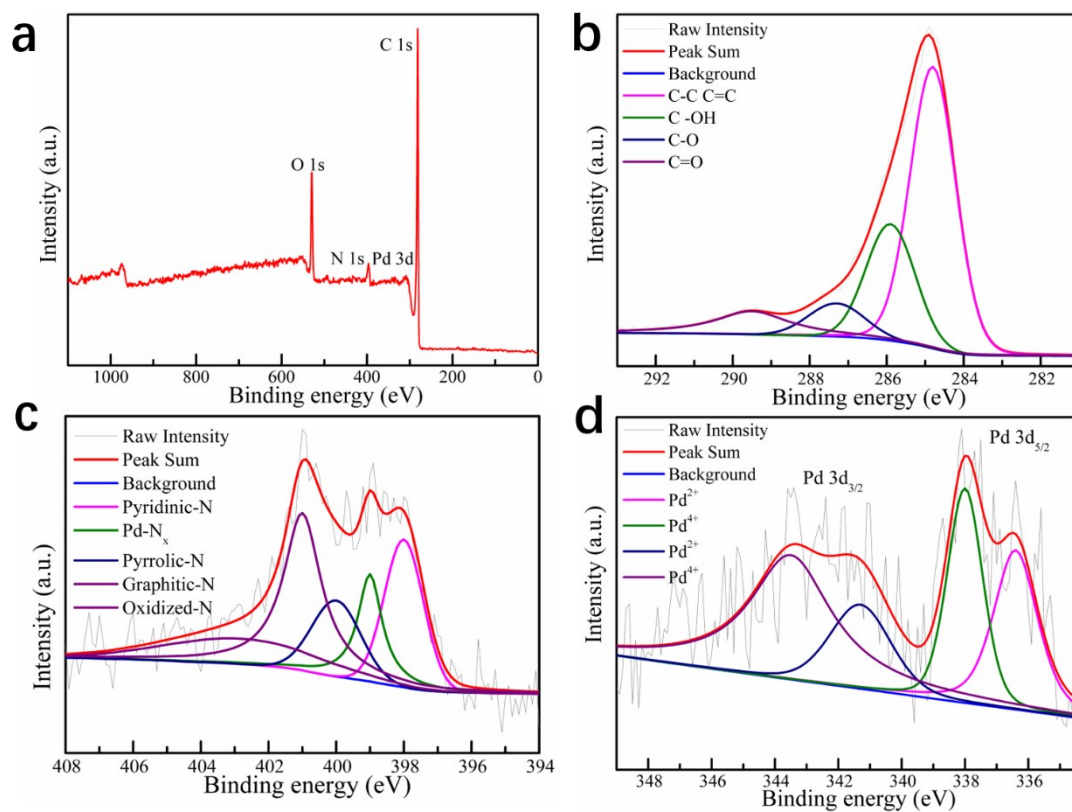


Fig. S14 (a) Survey, (b) C 1s, (c) N 1s and (d) Pd 3d spectra of the Pd/NCNSs.

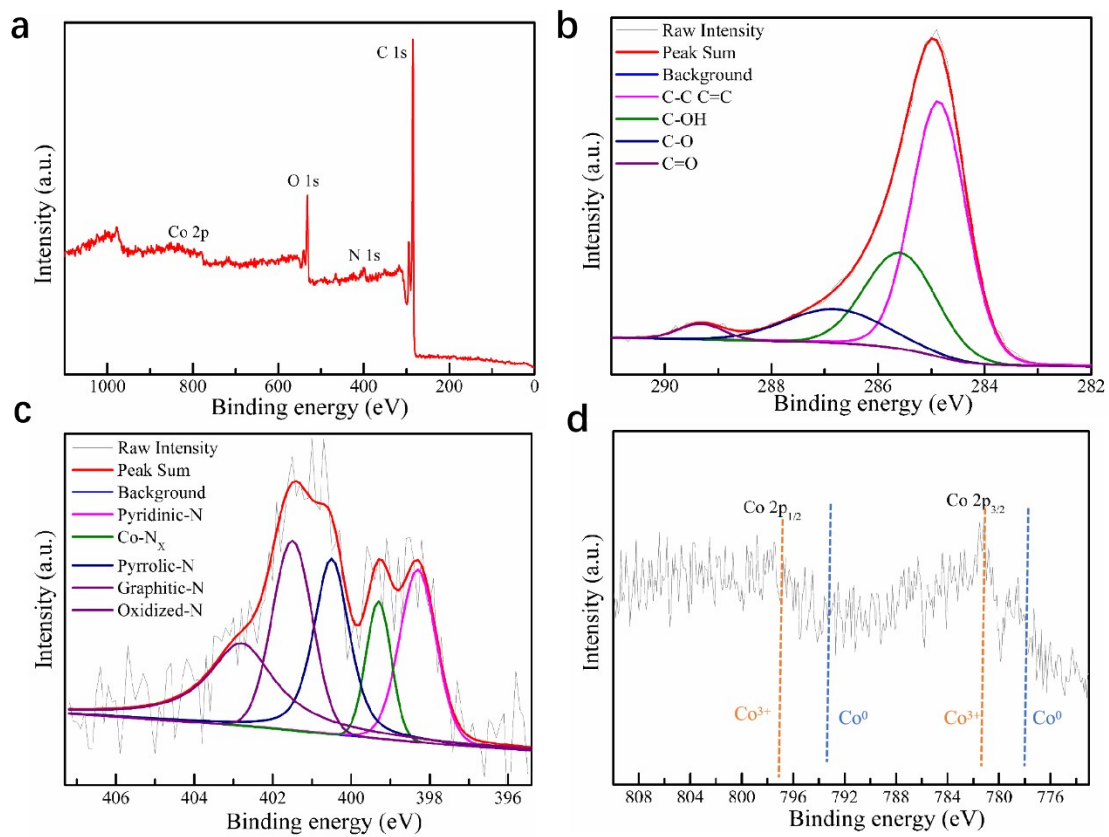


Fig. S15 (a) Survey, (b) C 1s, (c) N 1s and (d) Co 2p spectra of the Co/NCNSs.

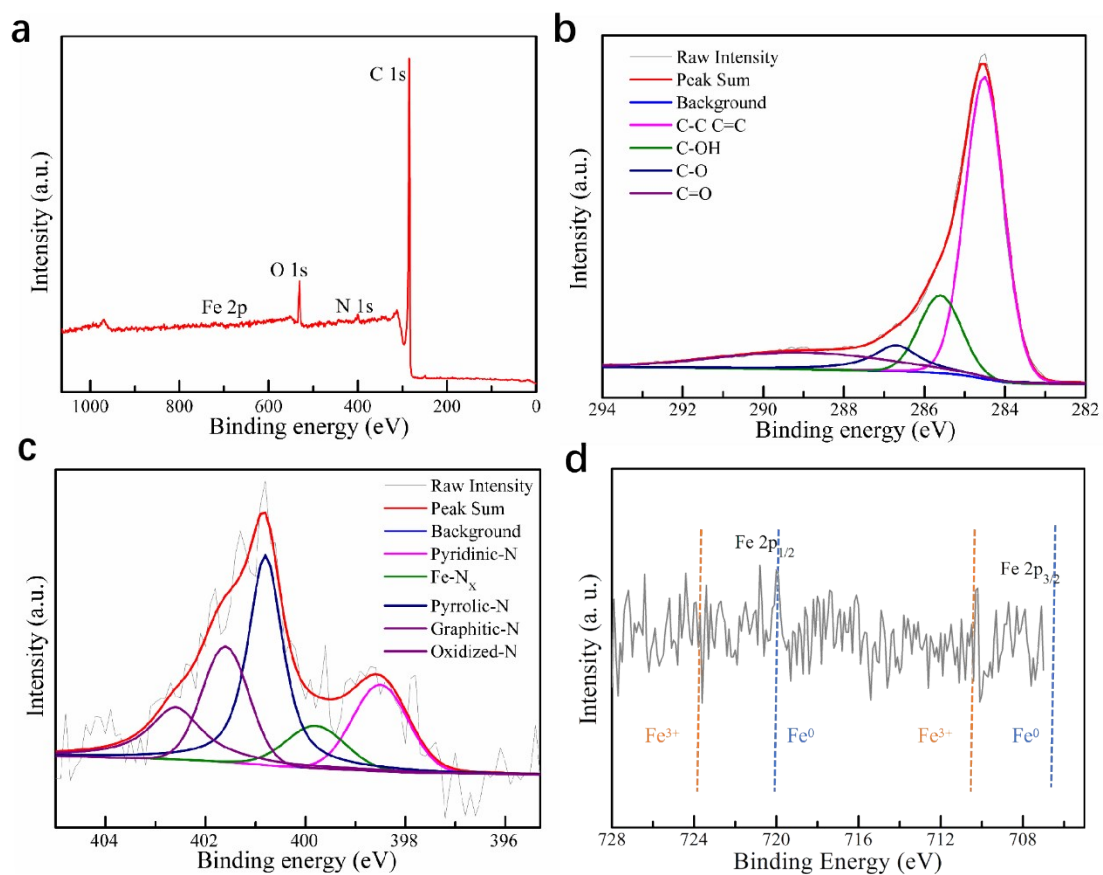


Fig. S16 (a) Survey, (b) C 1s, (c) N 1s and (d) Fe 2p spectra of the Fe/NCNSs.

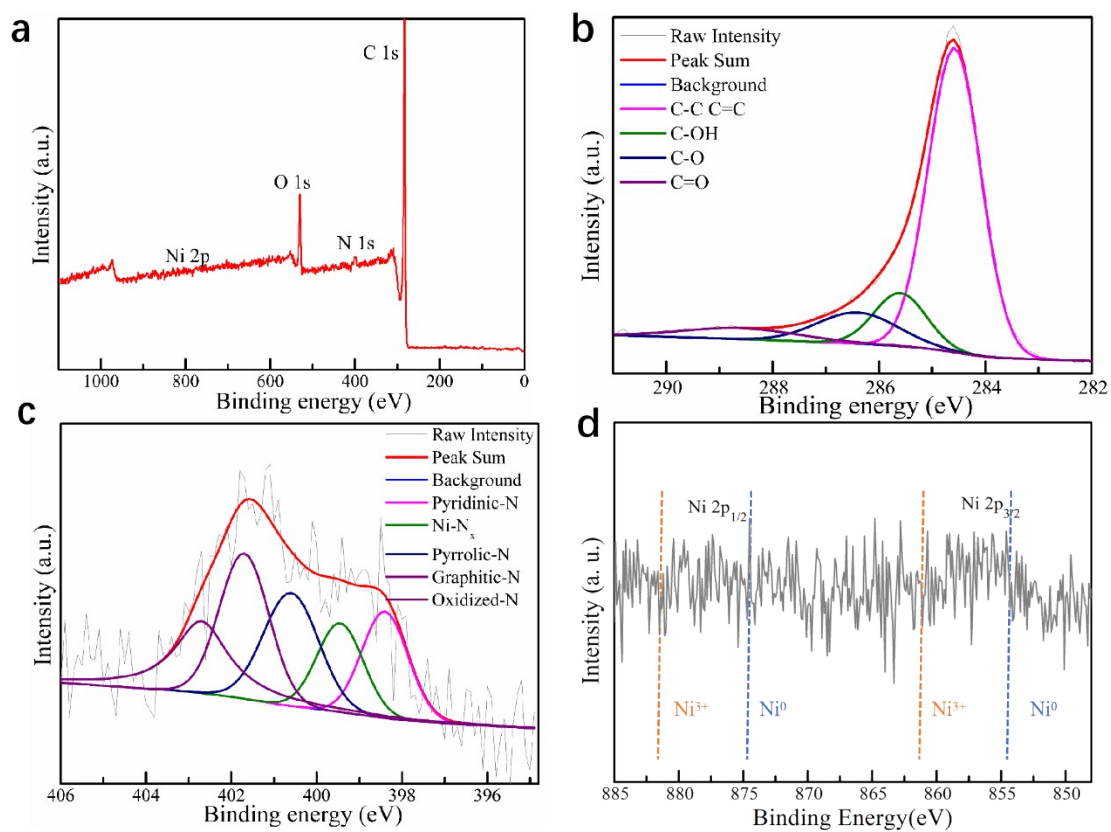


Fig. S17 (a) Survey, (b) C 1s, (c) N 1s and (d) Ni 2p spectra of the Ni/NCNSs.

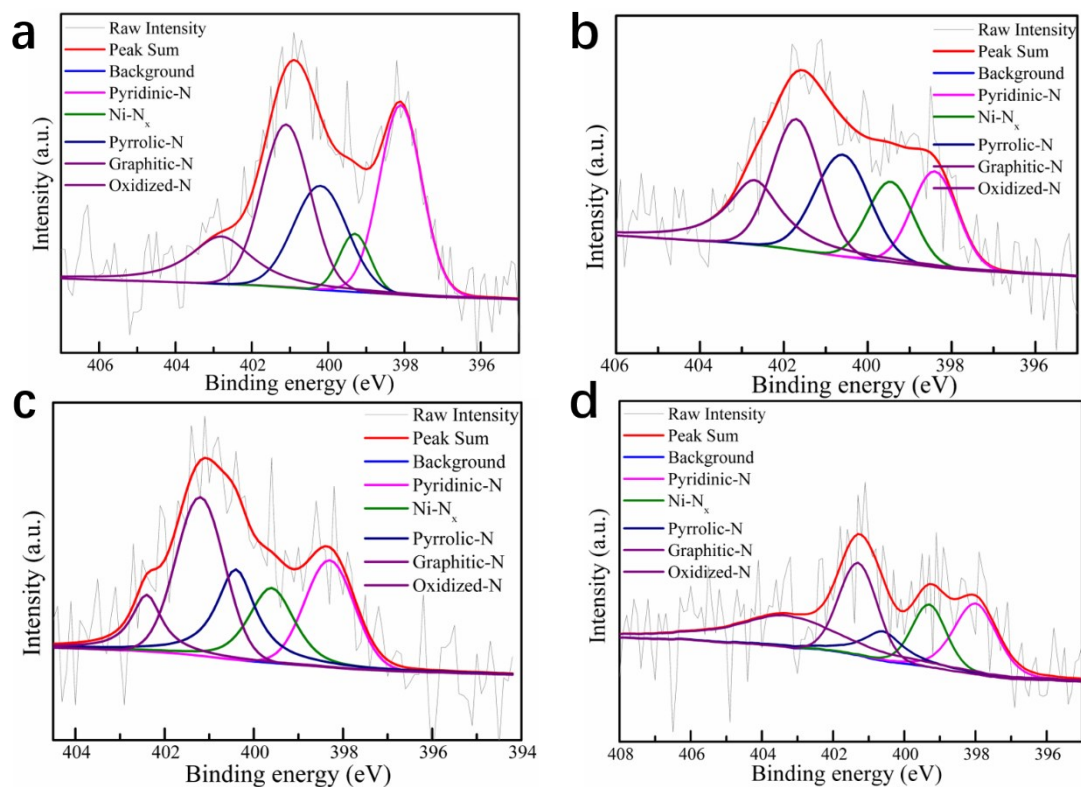


Fig. S18 N 1s spectra of the Ni/NCNSs samples prepared at (a) 800, (b) 900, (c) 1000 and (d) 1100 °C

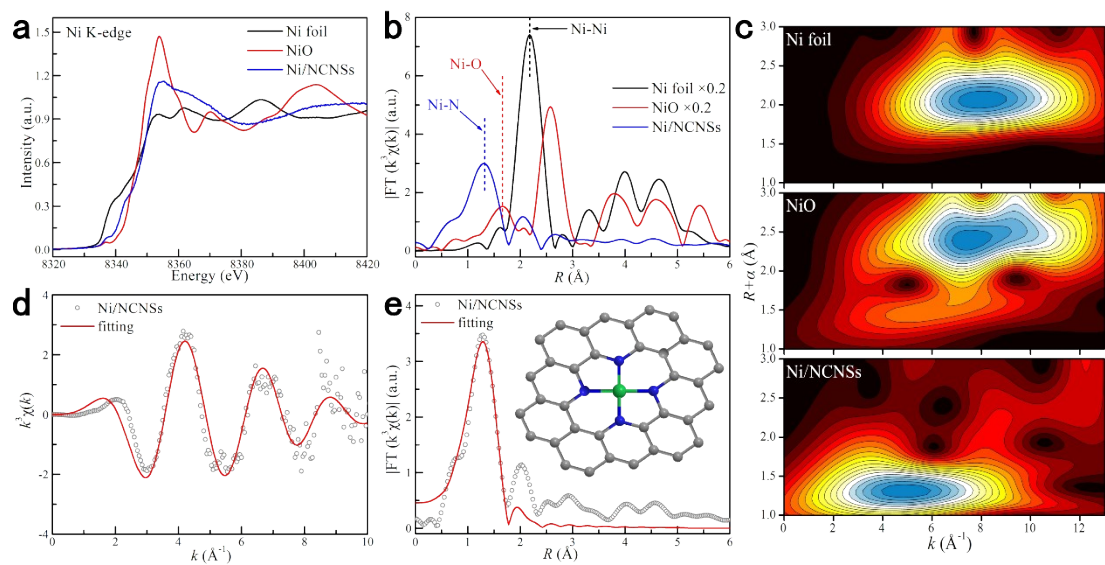


Fig. S19 Synchrotron XAFS measurement of Ni/NCNSs. (a) XANES spectra, (b) k^3 -weighted FT-EXAFS of Ni/NCNSs and references at Ni K-edge, (c) WT for the EXAFS signal of Ni/NCNSs and references, and (d, e) Corresponding EXAFS fitting curves in k and R space, respectively, inset displays the atomic structure model.

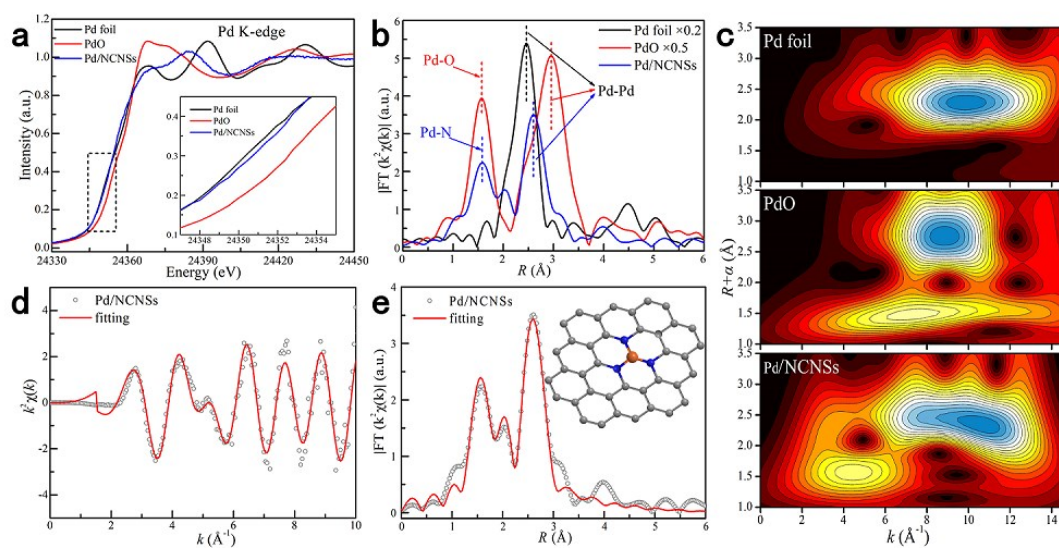


Fig. S20 Synchrotron XAFS measurement of Pd/NCNSs. (a) XANES spectra, (b) k^2 -weighted FT-EXAFS of Pd/NCNSs and references at Pd K-edge, (c) WT for the EXAFS signal of Pd/NCNSs and references, and (d, e) Corresponding EXAFS fitting curves in k and R space, respectively, inset displays the atomic structure model.

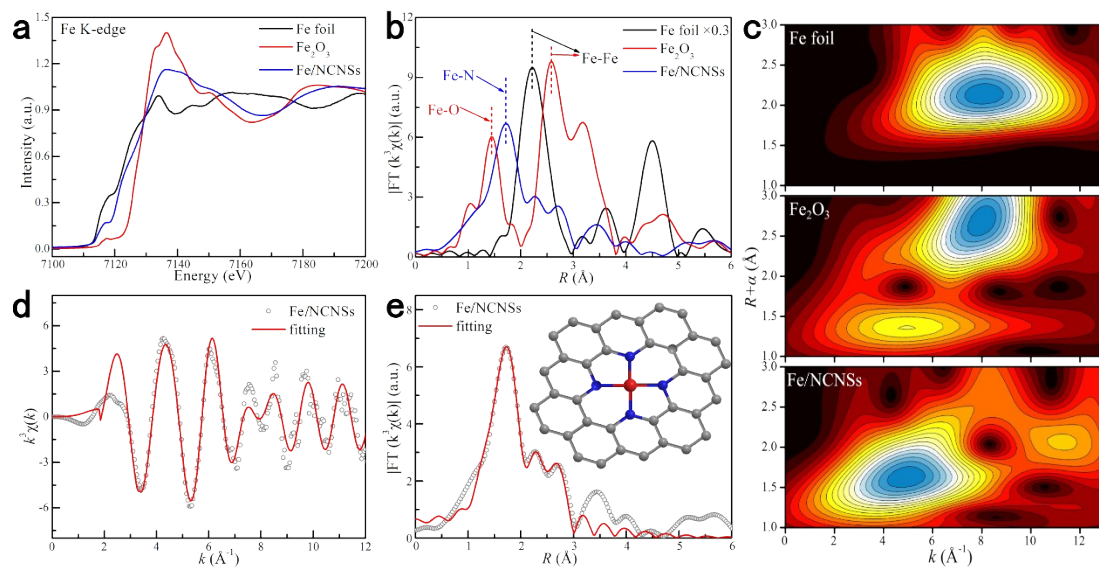


Fig. S21 Synchrotron XAFS measurement of Fe/NCNSs. (a) XANES spectra, (b) k^3 -weighted FT-EXAFS of Fe/NCNSs and references at Fe K-edge, (c) WT for the EXAFS signal of Fe/NCNSs and references, and (d, e) Corresponding EXAFS fitting curves in k and R space, respectively, inset displays the atomic structure model.

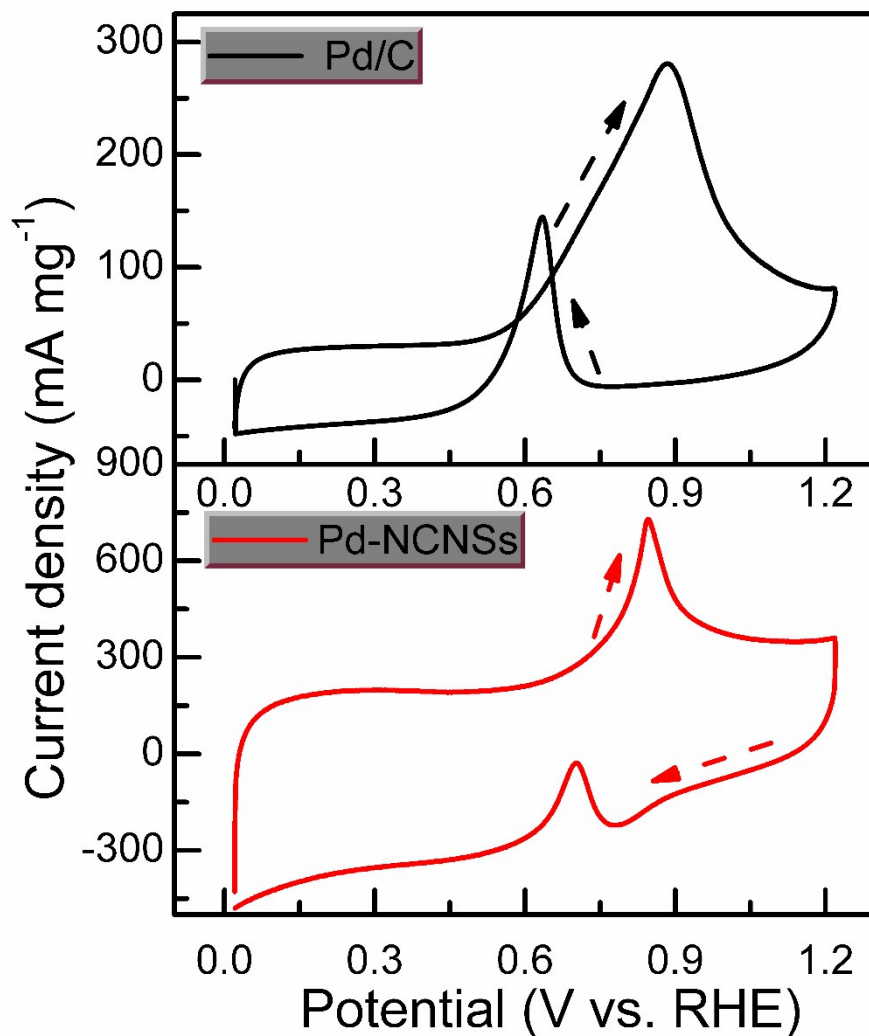


Fig. S22 Cyclic voltammetry curves of glycerol oxidation over the Pd/C and Pd/NCNSs catalysts.

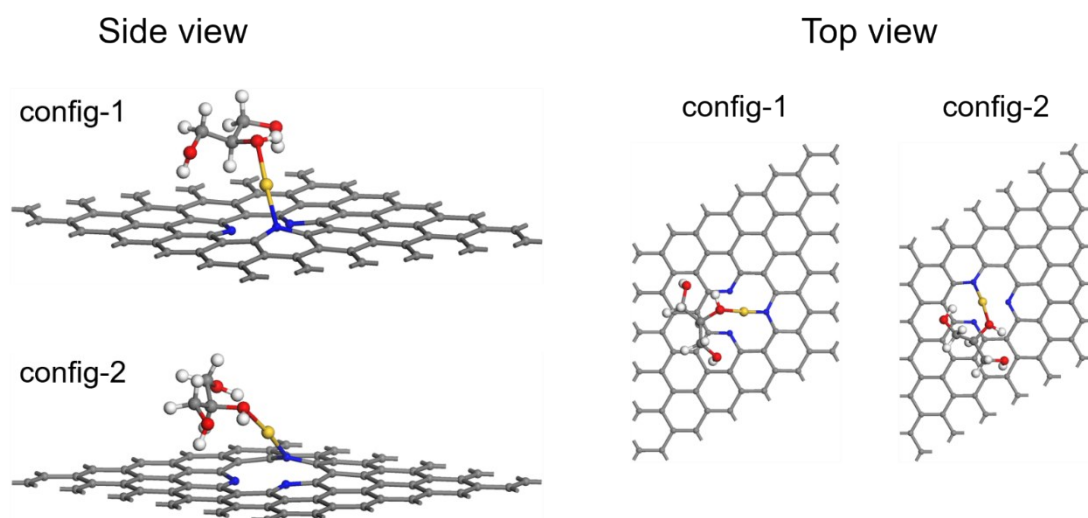


Fig. S23 Additional two adsorption configurations of glycerol molecules on single Au atom catalyst.

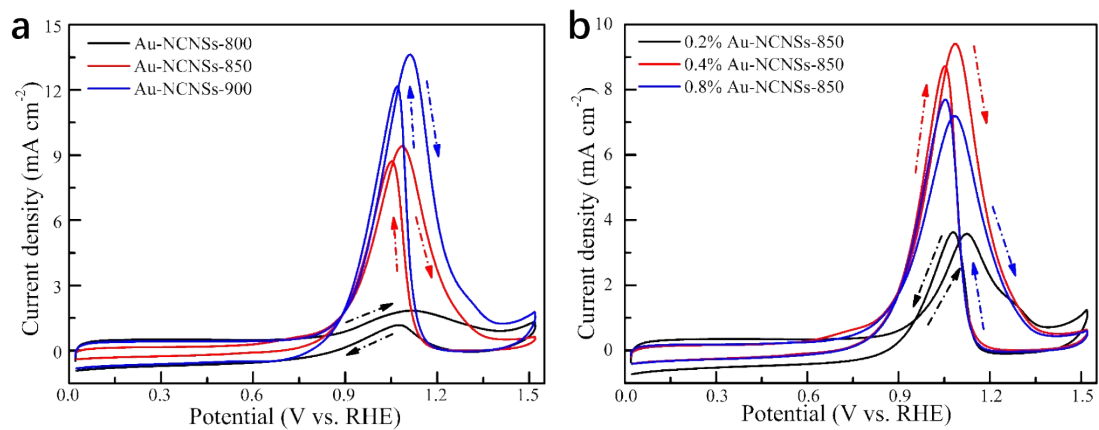


Fig. S24 Cyclic voltammetry curves of glycerol oxidation over the Au/NCNSs prepared with (a) varying pyrolysis temperatures and (b) varying concentrations of Au precursor.

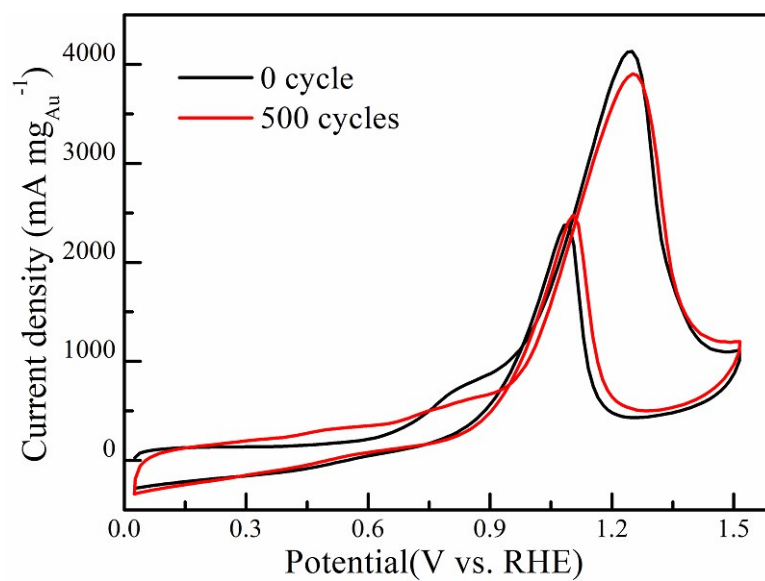


Fig. S25 Cyclic voltammetry curves of glycerol oxidation over the Au/NCNSs before and after 500 cycles.

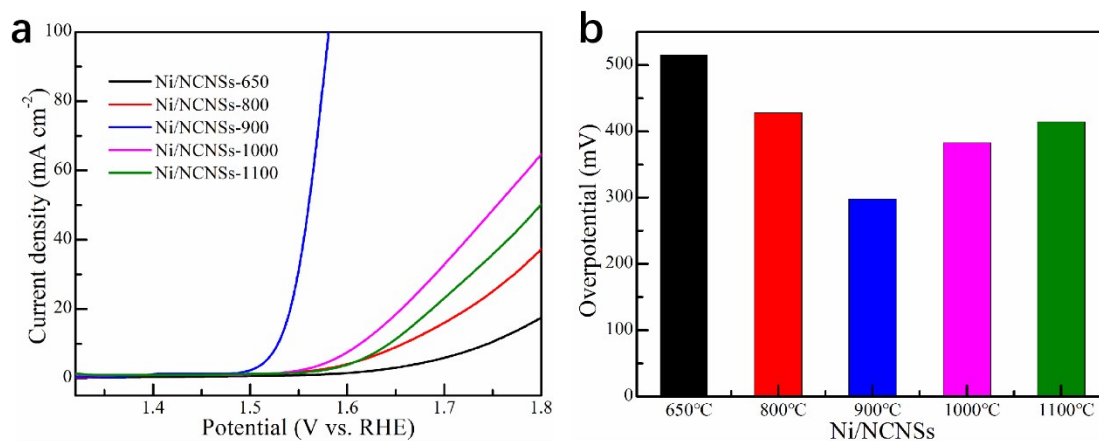


Fig. S26 (a) Polarization curves and (b) overpotentials at 10 mA cm⁻² of Ni/NCNSs prepared with varying pyrolysis temperatures. Catalysts were prepared with a cyanamide/furfural ratio of 1:1 and a metal loading (metal in feedstock) of 0.5 wt%.

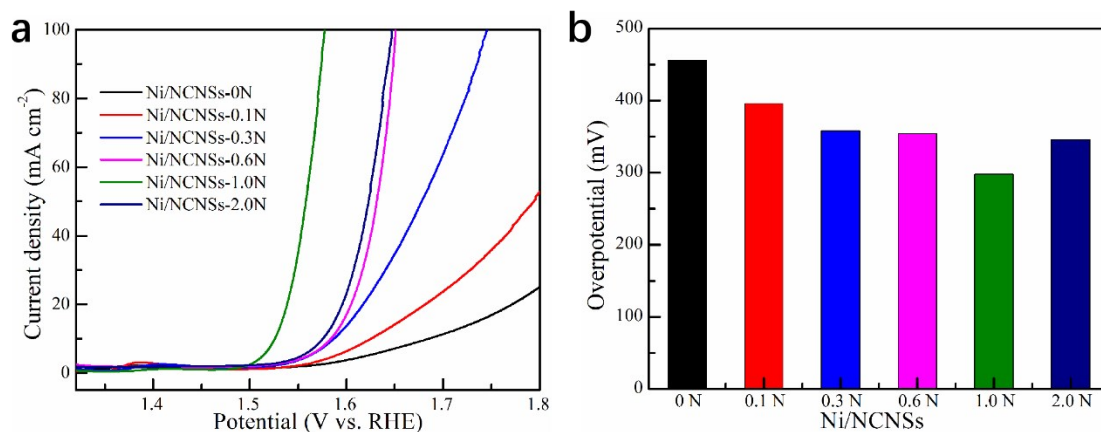


Fig. S27 (a) Polarization curves and (b) overpotentials at 10 mA cm^{-2} of Ni/NCNSs with varying concentrations of nitrogen precursor in the feedstock. Catalysts were prepared with a pyrolysis temperature of 900°C and a metal loading (metal in feedstock) of $0.5 \text{ wt}\%$

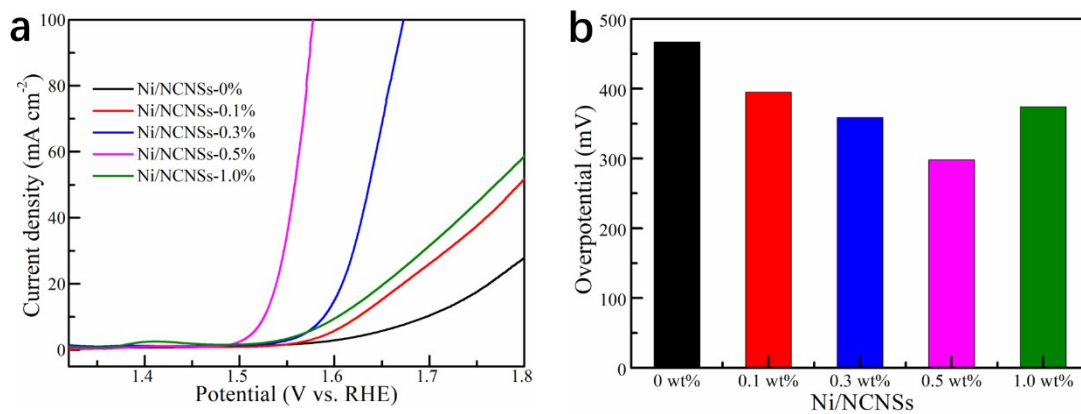


Fig. S28 (a) Polarization curves and (b) overpotentials at 10 mA cm⁻² of Ni/NCNSs with varying concentrations of metal precursor in the feedstock. Catalysts were prepared with a cyanamide/furfural ratio of 1:1 and a pyrolysis temperature of 900°C.

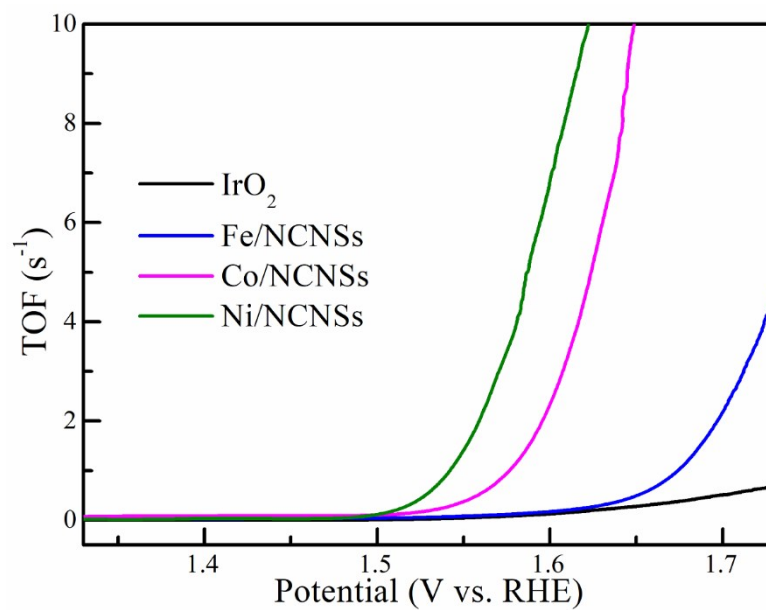


Fig. S29 TOF values of the catalysts for the OER

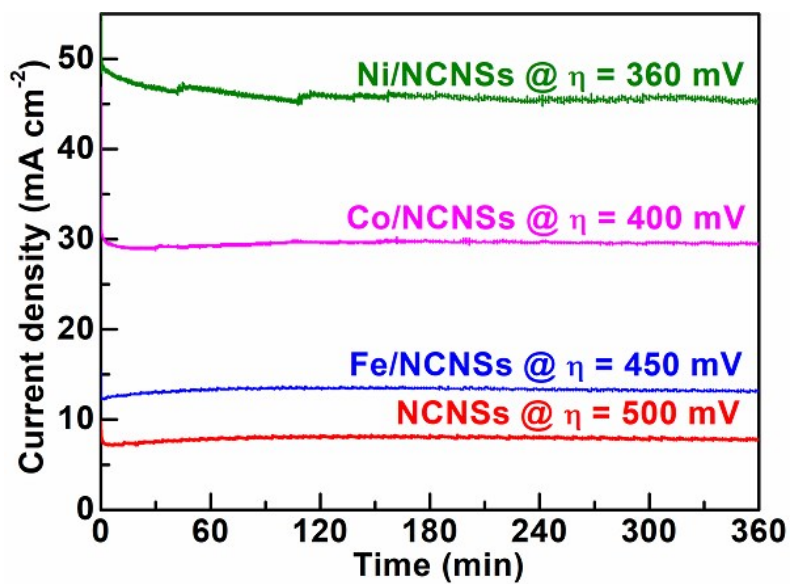


Fig. S30 chronoamperometric curves of the NCNSs, Fe/NCNSs, Co/NCNSs and Ni/NCNSs recorded at varying potential.

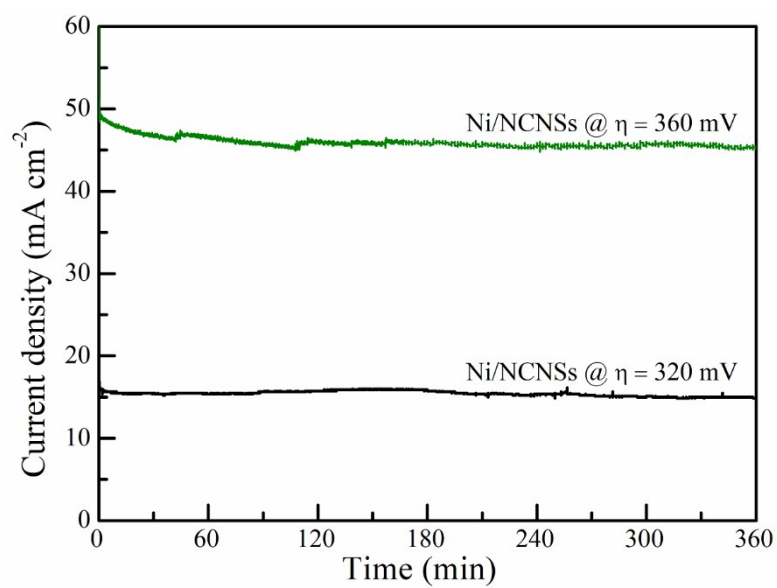


Fig. S31 chronoamperometric curves of the Ni/NCNSs at potentials of 360 and 320 mV

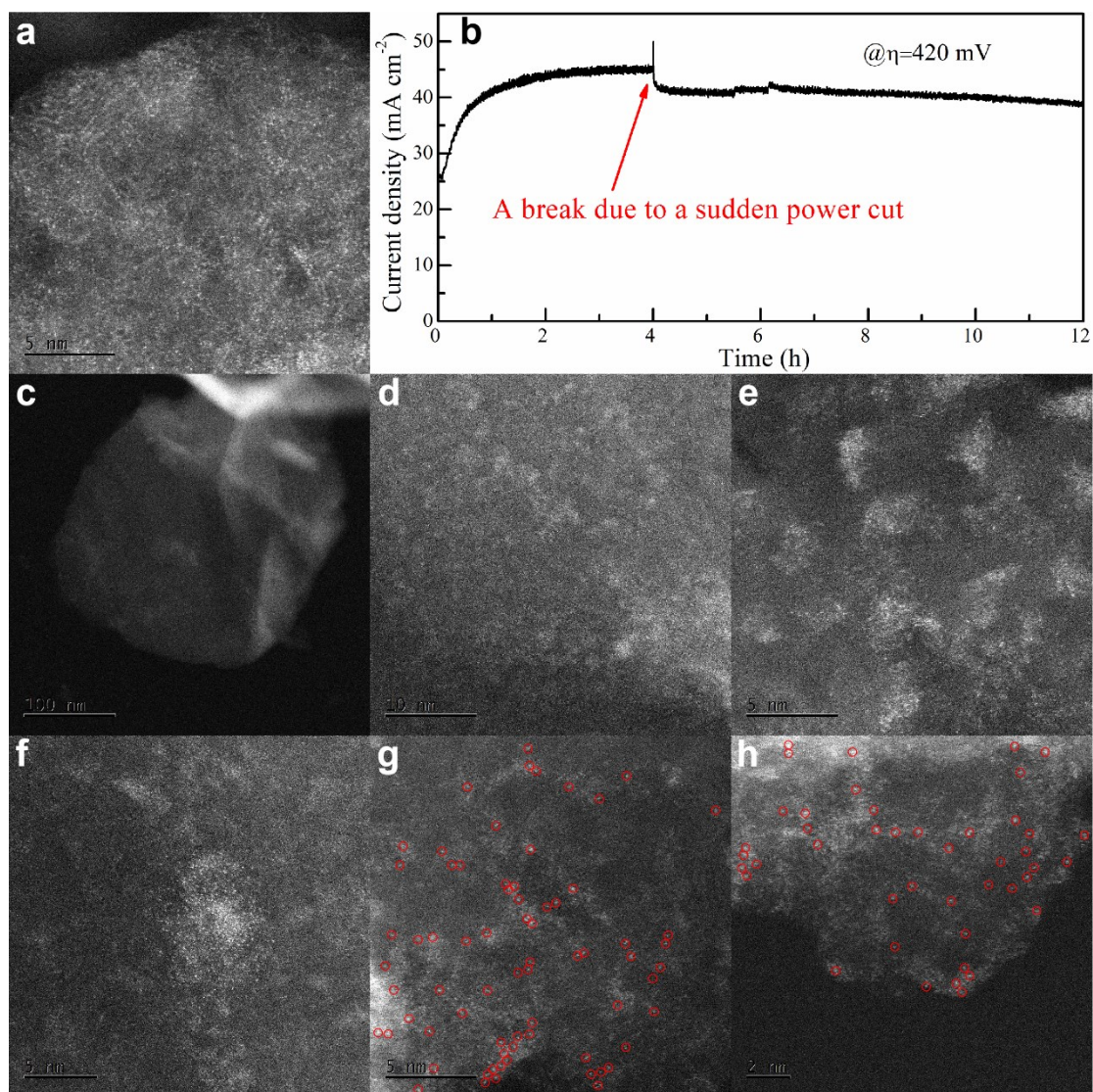


Fig. S32 Co/NCNSs sample before and after a 12 h chronoamperometric measurements. (a) HAADF-STEM image of fresh Co/NCNSs sample. (b) Chronoamperometric curves of Co/NCNSs at an overpotential of 420 mV, the nafion solution was not added during electrode preparation. (c-h) HAADF-STEM images of spent Co/NCNSs sample, the single cobalt atoms are highlight by red cycles.

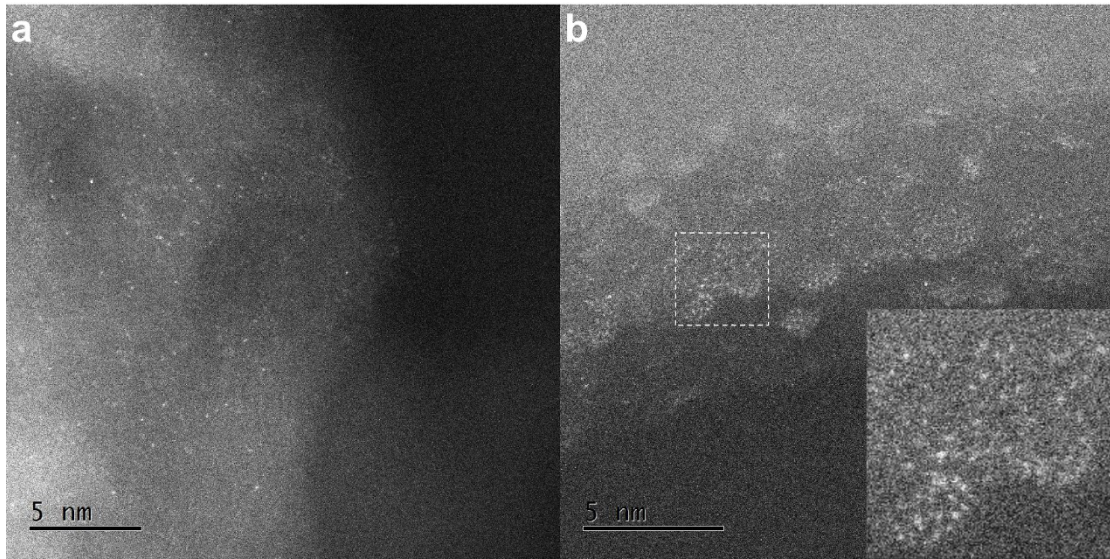


Fig. S33 HAADF-STEM images of Au/NCNSs sample after 1000 cycles for glycerol electro-oxidation.

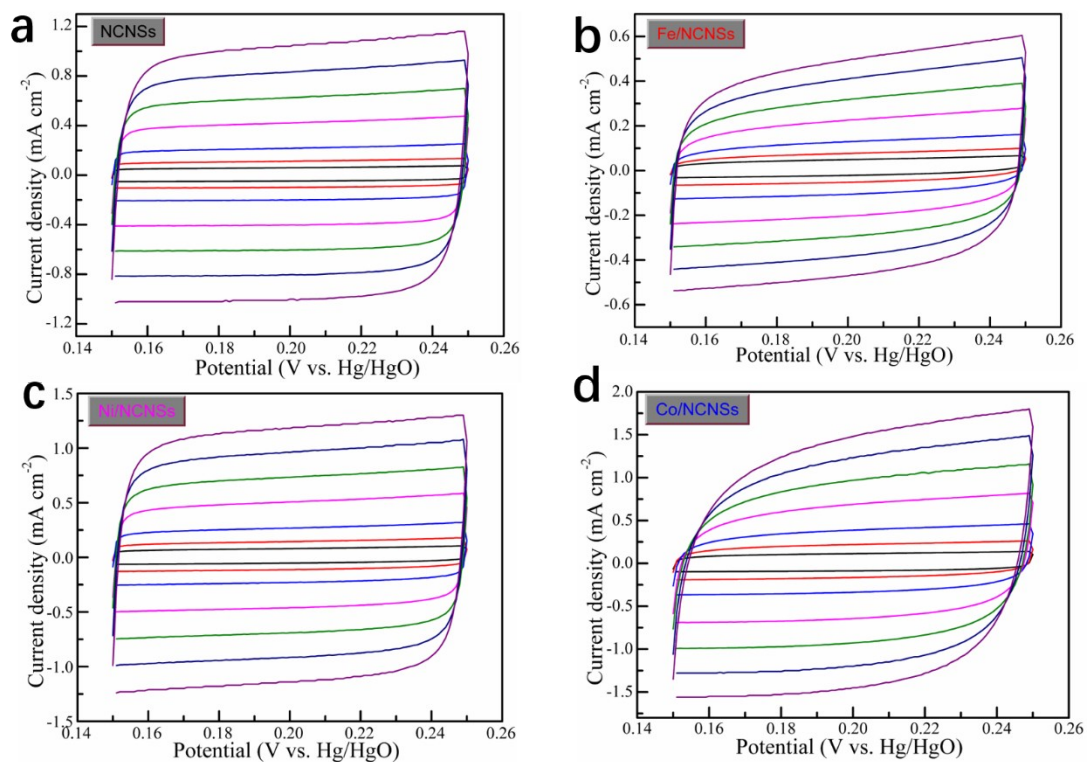


Fig. S34 Cyclic voltammetry curves of (a) NCNSs, (b) Fe/NCNSs, (c) Ni/NCNSs and (d) Co/NCNSs with scan rates of 5 (Black line), 10 (Red line), 20 (Blue), 40 (Magenta), 60 (Olive line), 80 (Navy line) and 100 mV s⁻¹ (Violet line)

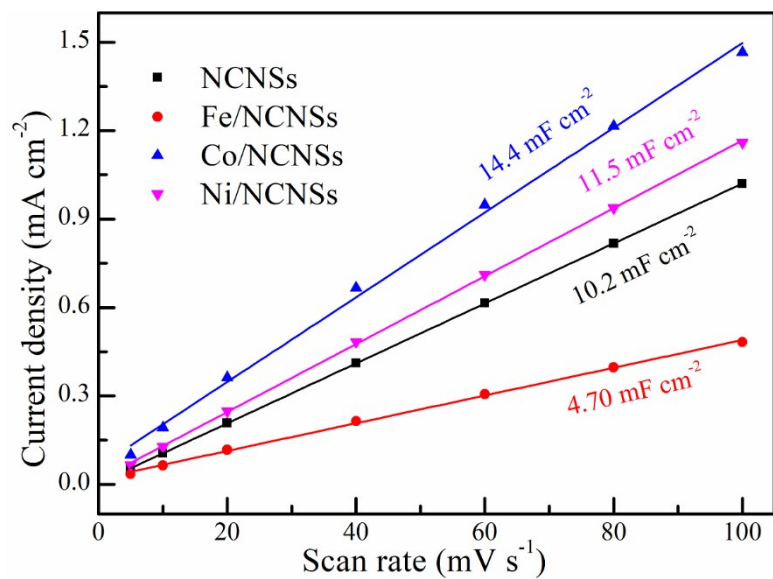


Fig. S35 Dependence of $(j_a - j_c)/2$ on the scan rate of the samples.

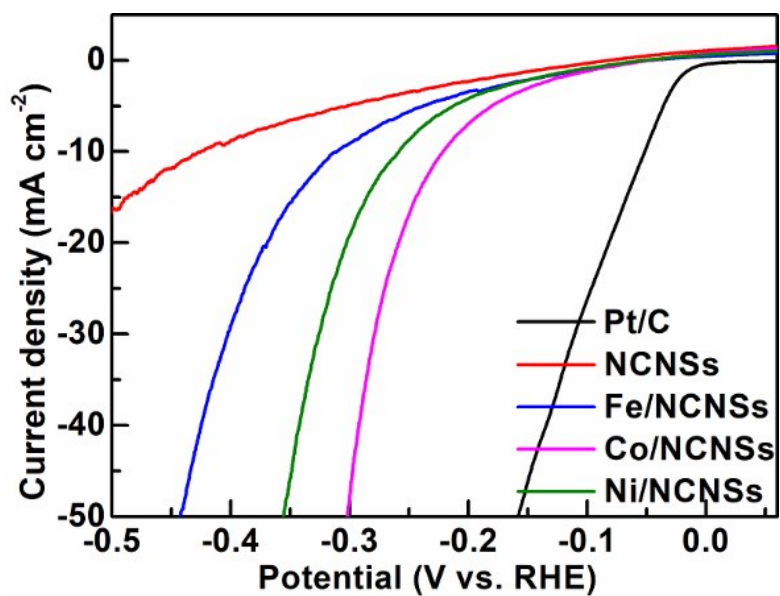


Fig. S36 HER polarization curves recorded in a solution of 1 M KOH with a scan rate of 2 mV s⁻¹,

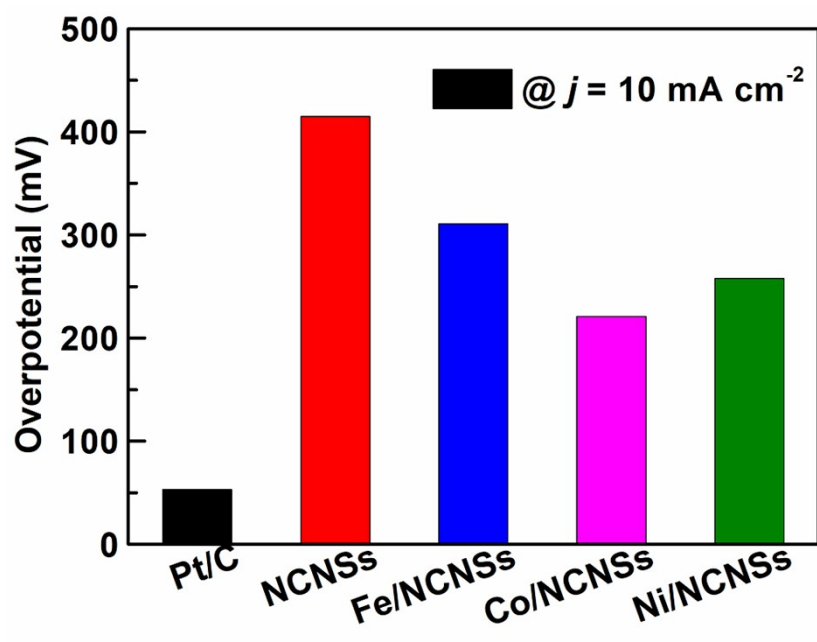


Fig. S37 Comparison on overpotentials at a HER current density of 10 mA cm^{-2}

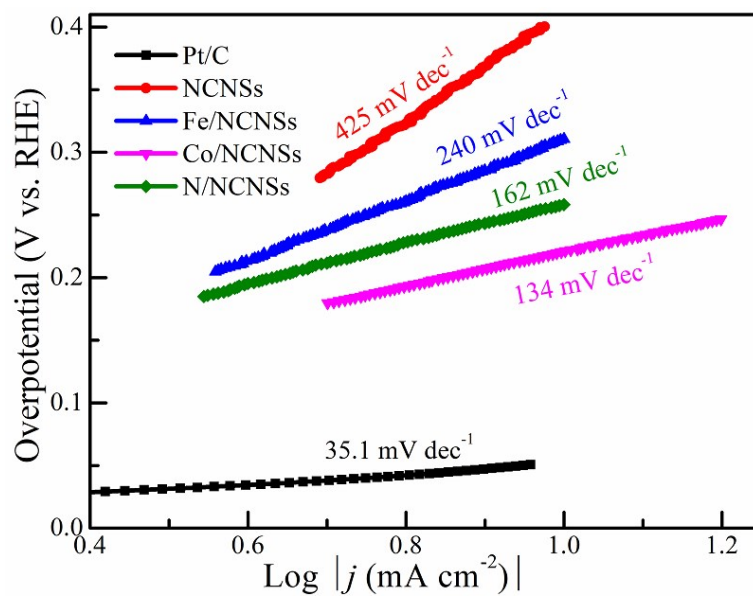


Fig. S38 Tafel slopes of the catalysts for the HER.

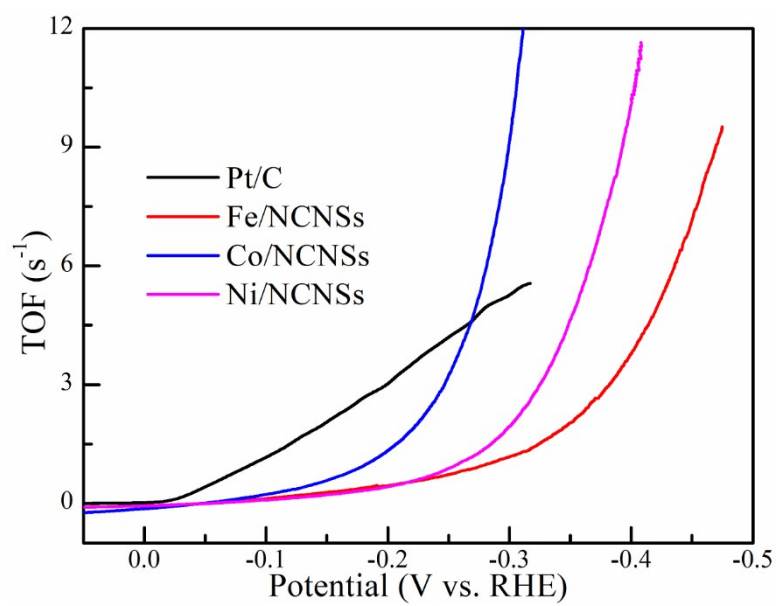


Fig. S39 TOF values of the catalysts for the HER

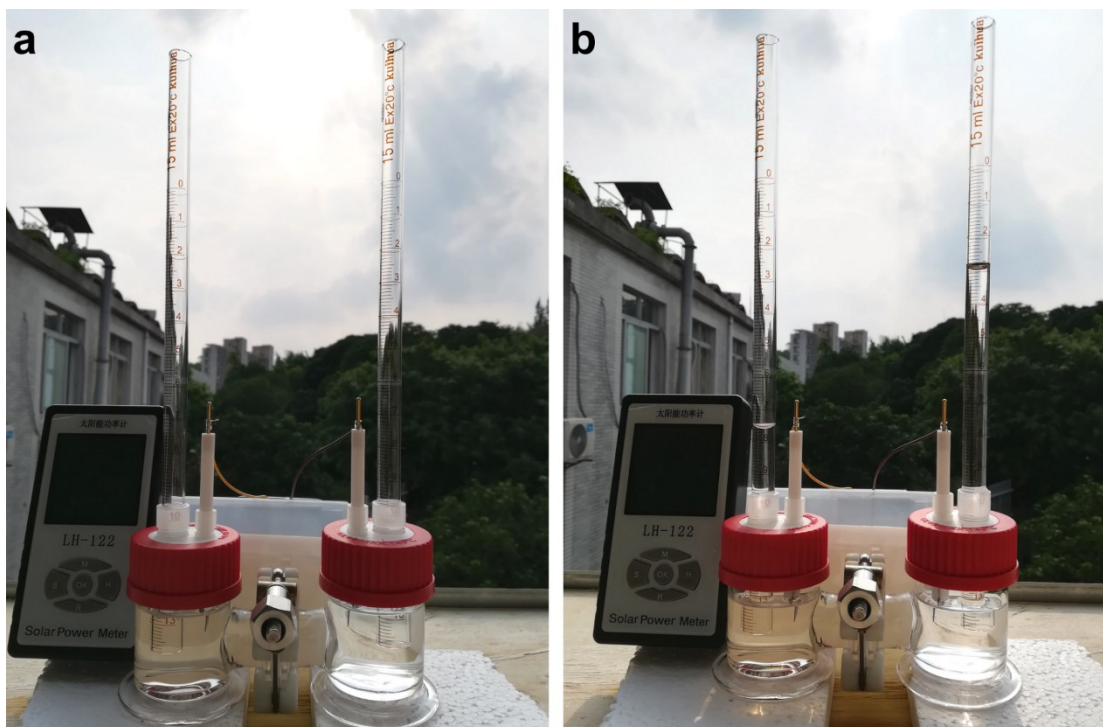


Fig. S40 digital photos of a solar panel powered set-up (a) before and (b) after electrolysis for 2130 seconds, respectively

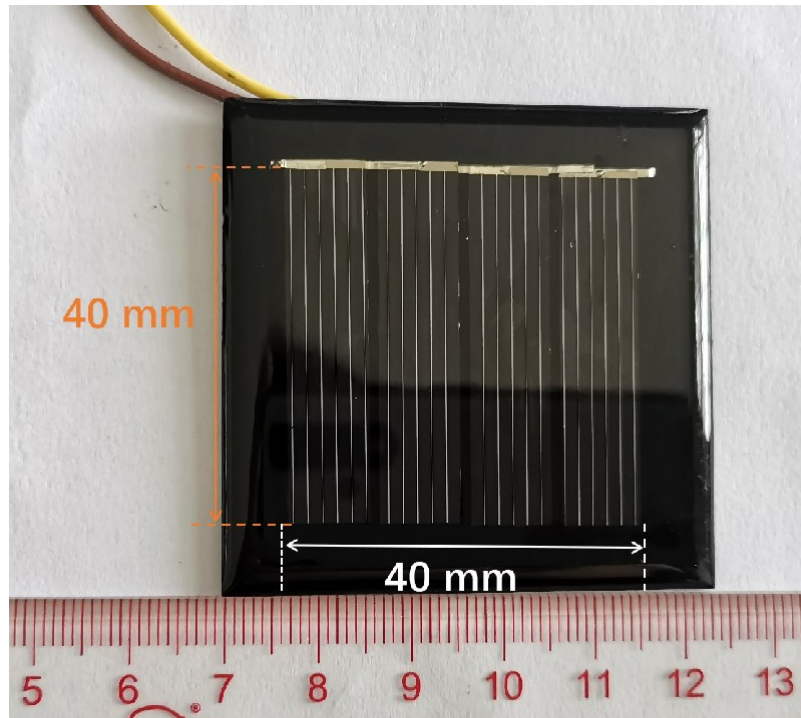


Fig. S41 Digital photo of a 2.0 V solar panel. The effective area of the solar panel is 40×40 mm.

References

- [1] Y.R. Xue, B.L. Huang, Y.P. Yi, Y. Guo, Z.C. Zuo, Y.J. Li, Z.Y. Jia, H.B. Liu, Y.L. Li, Anchoring zero valence single atoms of nickel and iron on graphdiyne for hydrogen evolution. *Nat. Commun.* **2018**, *9*, 1460.